Micromechanical detectors for ferromagnetic resonance spectroscopy

John Moreland,[a] Pavel Kabos,[a] Albrecht Jander, [a] Markus Löhndorf, [b]
Robert McMichael,[c] and Chan-Gyu Lee[c]

[a]National Institute of Standards and Technology, Mail Stop 814.05, Boulder, CO 80303
[b]Center of Advanced European Studies and Research (CAESAR), Bonn, Germany
[c]Metallurgy Division, National Institute of Standards and Technology, Gaithersburg, MD

ABSTRACT

We demonstrate micromechanical detection of ferromagnetic resonance (FMR) in thin magnetic films. FMR spectroscopy is performed on nanometer scale samples integrated with a micromachined silicon cantilever. We present several techniques by which the FMR signal is coupled to a mechanical response of the cantilever. Cantilevers with low spring constants and high mechanical Q are essential for these measurements. Sub-nanometer displacements of the cantilever are detected using a laser beam-bounce system typical of many atomic force microscopes (AFM). The high sensitivities achieved by integrating the sample with the detector allow magnetic measurements on samples with total magnetic moments smaller than detectable with conventional magnetometers. Metrology applications for micromachined magnetometers include ultra-thin film material characterization, magnetic field microscopy, microwave field imaging, and deposition process monitors.

Keywords: MEMS, Micromechanical detector, Ferromagnetic resonance (FMR), M-H loops, Bimaterial calorimeter, Torque magnetometer, Atomic force microscope (AFM), Microwave instrumentation.

1. INTRODUCTION

1.1 Motivation

The characterization of nanometer-scale magnetic multilayer films, patterned recording media, and magnetic devices has proven to be a challenge for conventional magnetometers. The limitation on sensitivity stems from low sample-volume/sensor-volume ratios typical of conventional magnetometers. Sensitivity can be improved tremendously by integrating samples with the measurement transducer using microfabrication methods. In particular, we are developing a new class of magnetometer based on microelectromechanical systems (MEMS) for measuring magnetic forces and torques on samples deposited onto microscopic flexible structures.

As an example, consider the simple MEMS sensor having a thin magnetic film deposited onto a micromachined torsional oscillator (Fig. 1). When the oscillator is excited resonantly by an external ac magnetic field, its angular displacement is proportional to the magnetic moment of the film. We refer to this device as a "micro resonating torque magnetometer" or μRTM. In principle, a torque as small as 10^{-20} N·m can be detected at room temperature by measuring the resonant frequency shift of the oscillator caused by changes in the magnetic moment of the film. In contrast, the best torque sensitivity for conventional instruments is 10^{-10} N·m.

Several authors have investigated similar MEMS-based magnetometers over the last ten years.[1-7] In this paper, we focus on some of the microcantilever configurations recently studied in our laboratories that demonstrate the usefulness of MEMS magnetometers. MEMS magnetometers allow accurate measurements of isolated thin-film samples with nanometer dimensions under ambient conditions. In addition, batch-fabrication of MEMS magnetometers has potential as a cost-effective method for measuring the magnetic properties of small samples and devices.

1.2 Mechanical torque on a thin magnetic film

The magnetization M in a magnetic film will generate a mechanical torque T in the presence of an applied torque field H_T (see Fig. 2). In many cases, thin-film shape anisotropy is sufficient to generate mechanical torques that can be measured with

e-mail – moreland@boulder.nist.gov

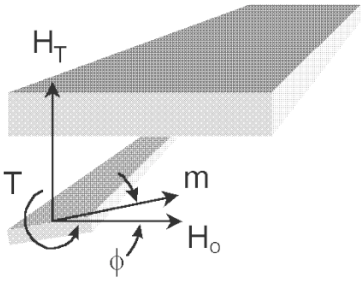

Fig. 1. Configuration for measuring the magnetic moment of a thin film deposited onto a microcantilever.

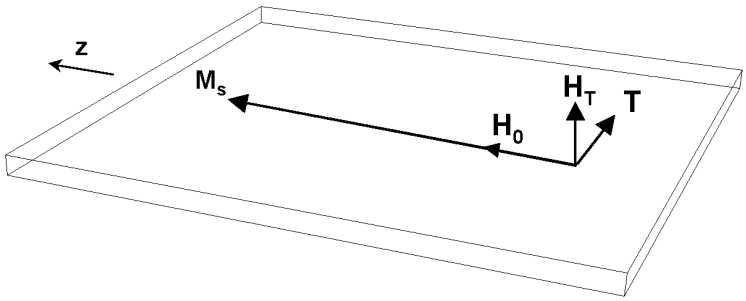

Fig. 2. Vector diagram showing the orientations of the magnetic fields and torque on a thin film magnetized in-plane along the z direction.

micromachined detectors. In particular, measuring T allows the determination of the saturation magnetization M_s when a sufficiently large field H_o is applied in the plane of the film: $T = \mu_o |\boldsymbol{M_s} \times \boldsymbol{H_T}| V = \mu_o M_s H_T V$, where V is the volume of the film (given that the angle between the plane of the film and $\boldsymbol{H_T}$ is set to 90°).[8] A practical limit for H_T is the field strength required to rotate the in-plane magnetization by 5° into the out-of-plane orientation. Below this limit, the in-plane magnetization is within 1 % of its value at $H_T = 0$. The in-plane and out-of-plane anisotropy fields for a given ferromagnetic material and a given geometry determine this field strength. For example, for polycrystalline Fe films thicker than 10 nm, field values on the order of 800 kA/m are necessary to rotate the magnetization 5° out-of-plane. For thinner films this field value can be reduced due to an increase in out-of-plane anisotropy.[9] For a 10 nm thick Fe film 50 μm wide by 450 μm long ($m = 2.4 \times 10^{-10}$ A·m^2) with $H_T = 90$ A/m we calculate $T = 2.7 \times 10^{-14}$ N·m.

If the magnetic film is deposited onto a microcantilever, then in principle, we can compute the torque knowing the geometric parameters of the cantilever. For small twist angles φ, $T = k\varphi$, where k is the torsional spring constant. According to elastic theory,[10,11]

$$k = \frac{wt^3 E}{6l(1+n)}, \tag{1}$$

where E is the Young's Modulus, n is the Poisson ratio, t is the thickness, w is the width, and l is the length of the cantilever. The signal-to-noise (SNR) is limited ultimately by the Brownian motion of the cantilever. Generally, sensitivity can be improved by operating at the cantilever resonance frequency, in vacuum, and at low temperatures.[12,13] However, we point out that it is possible to operate at room temperature, in air, and off resonance, and still achieve a magnetic-moment sensitivity on the order of 10^{-12} A·m^2.

1.3 Mechanical detection of ferromagnetic resonance (FMR)

1.3.1 Ferromagnetic resonance review

The dynamics of the magnetization of a ferromagnet is described by the Landau-Lifshitz-Gilbert equation

$$\frac{d\boldsymbol{M}}{dt} = \gamma(\boldsymbol{M} \times \boldsymbol{H}) + \frac{\alpha}{M_s}\left(\boldsymbol{M} \times \frac{d\boldsymbol{M}}{dt}\right), \tag{2}$$

where M is the magnetization, H the effective magnetic field, and γ the gyromagnetic ratio. The phenomenological damping factor α is referred to as the Gilbert term and is related to the spin-orbit coupling. In a static magnetic field, eq. 2 describes a precessional motion of the magnetization decaying from its initial direction until it lines up with the applied field, as shown in Fig. 3. In a typical FMR experiment, the sample is magnetized by a dc bias field H_o while a much smaller oscillating field H_1 is applied perpendicular to H_o. FMR occurs when H_1 oscillates at the natural precessional frequency of M. The driven FMR response is a continuous precession of the magnetization vector about H_0. The resonant frequency is determined by γ and H_0 and typically lies in the microwave range. Under FMR conditions, there is a peak in the power absorbed by the

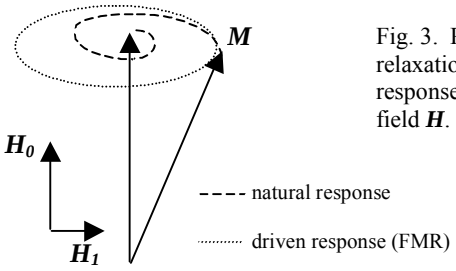

Fig. 3. Precession and relaxation of ***M*** in response to an applied field ***H***.

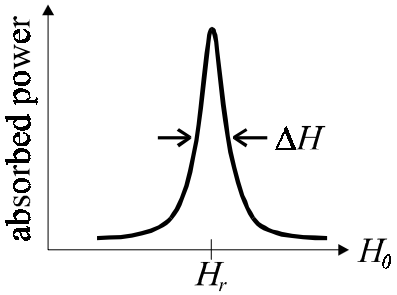

Fig. 4. Lorentzian absorption line typical of FMR showing power absorption as a function of swept bias field.

magnetic system as shown in Fig. 4. FMR is generally used to measure the magnetization, but it can also be used as sensitive probe of other internal fields due to magnetic anisotropy.

The effective saturation magnetization M_{eff} (including anisotropy terms), the damping factor α, and the imaginary part of the susceptibility χ'' (at resonance), can be determined from the FMR spectrum using the following relationships for a thin-film sample geometry in SI units.[14,15]

$$M_{eff} = \frac{1}{H_r}\left(\frac{\omega^2}{\gamma^2} - H_r^2\right), \tag{3}$$

$$\alpha = \frac{\gamma}{2\omega}\Delta H, \tag{4}$$

$$\chi'' = \frac{M_s}{\alpha}\frac{\gamma}{\omega}\left(\frac{M_{eff} + H_r}{M_{eff} + 2H_r}\right). \tag{5}$$

Here, $H_o = H_r$ at resonance, γ is the gyromagnetic constant, ΔH is the width of the resonance peak at half maximum as determined by the Lorentzian fit, and $\omega = 2\pi f$ is the microwave frequency. Note that $M_{eff} = M_s - 8\pi K_s/M_s t$ where M_s is the saturation magnetization, t is the film thickness, and K_s is the uniaxial surface anisotropy energy density parameter.[16] The uniaxial surface anisotropy term $8\pi K_s/M_s t$ is about 20 kA/m for a 30 nm ferromagnetic film and is negligible to first order compared to M_s for these measurements. We therefore assume $M_{eff} = M_s$ for the data presented here.

1.3.2 FMR based on a μRTM

The change in the mechanical torque under FMR conditions for a thin film is given by

$$\Delta T_{FMR} = \mu_0 \Delta M_z H_T V, \tag{6}$$

where ΔM_z is the change in the magnetization due to the FMR precession (see Fig. 5). For thin magnetic films, M_z can be calculated as [17,18]

$$M_z = \sqrt{M_s^2 - \left|m_{in}^2\right| - \left|m_{out}^2\right|} \approx M_s - \frac{\left|m_{in}^2\right| + \left|m_{out}^2\right|}{2M_s}, \tag{7}$$

where M_s is the saturation magnetization, m_{in} the in-plane component of the dynamic magnetization and m_{out} the out-of-plane component of the dynamic magnetization. For $\Delta M_z = M_s - M_z$ we see that

$$\Delta M_z = \frac{\left|m_{in}^2\right| + \left|m_{out}^2\right|}{2M_s} = \frac{\left|m_{in}^2\right|}{2M_s}\left(1 - \left|\frac{m_{out}}{m_{in}}\right|^2\right). \tag{8}$$

For a microwave field $H_1 << M_s$ we can neglect the second term of (8) since the ratio

$$\left|\frac{m_{out}}{m_{in}}\right|^2 = \frac{H_r}{H_r + M_s}, \tag{9}$$

and so ΔM_z becomes

$$\Delta M_z = \frac{\left|m_{in}^2\right|}{2M_s} \approx \frac{\left(H_1 \chi''\right)^2}{4M_s}, \tag{10}$$

given that $\left|m_{in}\right| \approx H_1 \chi''$ for small FMR tilt angles.

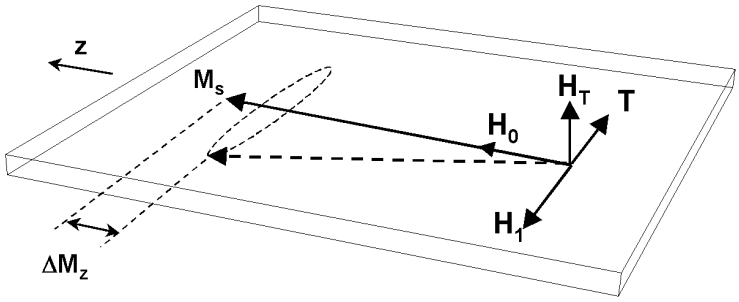

Fig. 5. Vector diagram showing the orientation of the applied fields and mechanical torque generated in an FMR experiment.

Damping causes the precessional motion of the magnetization m to lag the oscillating microwave magnetic field H_1. A component of m is out of phase with H_1 and results in absorption of energy from the microwave field, as discussed above. The component of m that is in phase with H_1 and is perpendicular to it results in a torque. The case shown in Fig. 6 is for the 90º lag that occurs near resonance between circularly polarized microwaves and the rotating m vector. For circularly polarized microwaves, the torque is

$$T = \mu_o \left|m_{out}\right| H_{1in} + \mu_o \left|m_{in}\right| H_{1out}. \tag{11}$$

Here $H_{1\text{-}in}$ and $H_{1\text{-}out}$ are the in-plane and out-of-plane components of the microwave field. This is an important result that will impact metrology applications of MEMS magnetometers as discussed below.

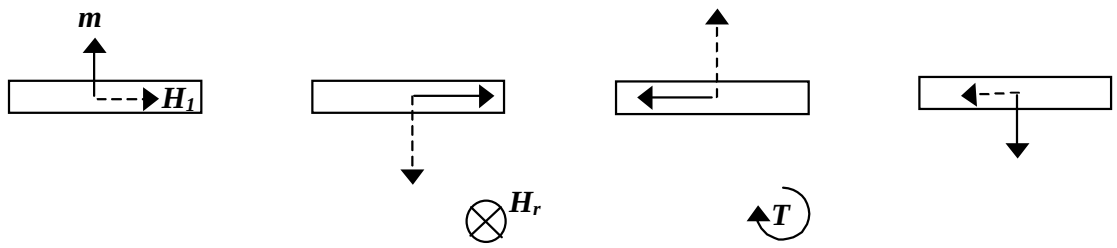

Fig. 6 Diagram showing the time progression of the circularly polarized microwave field H_1 and the precessing magnetization m at resonance. The bias field H_r is directed into the page. The lag between the motion of the magnetization and the driving field produces a torque as indicated.

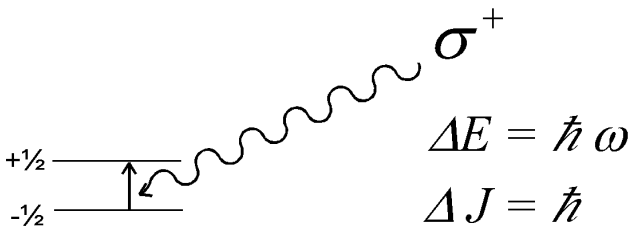

Fig. 7. Spin transitions can also be described in a quantum picture that conserves both energy and angular momentum.

It is interesting to note that spin transitions must conserve energy and angular momentum. Consider the simple diagram in Fig. 7 where a circularly polarized photon with angular momentum $\hbar$ and energy $\hbar\omega$ generates a spin transition. The torque exerted on the system is $T = \hbar \cdot dN/dT$ and the power absorbed is $P = \hbar\omega \cdot dN/dT$, where dN/dt is the number of photons per second absorbed by the sample. Thus we see that $P_{res} = \omega T_{res}$. This is why we refer to this method as "angular momentum absorption" FMR.

1.3.3 FMR based on a bimaterial calorimeter

A bimaterial calorimeter for FMR can be understood within the mathematical framework developed for other bimaterial thermal sensors. Consider the silicon cantilever with its metallic coating as a rectangular beam fixed at one end comprised of two layers that have different thermal properties. Barnes *et al.*[19] solve the heat equation for this configuration and show that the deflection at the free end of the beam is

$$z = a\frac{E_1}{E_2}\frac{t_1^2 l^3}{t_2^3 w}\left(\frac{\gamma_1 - \gamma_2}{\lambda_1 t_1 + \lambda_2 t_2}\right)P, \tag{12}$$

where γ, λ, t , w, l, and E are respectively the thermal expansion coefficient, thermal conductivity, thickness, width, length, and Young's modulus of the beam layers (subscripts refer to the different materials) and P is the absorbed power. Equation (12) applies only in the limit $t_1 << t_2$ (t_1 is thickness of the magnetic film and t_2 is the thickness of the silicon cantilever). In addition, it is assumed that the temperature is constant over any cross section along the axis of the cantilever - this is a good approximation if t_1, $t_2 << l$. The constant a ranges from a value of 2, if power is absorbed near the end of the beam, to a value of 1.25, if power is absorbed uniformly along the beam.

There is significant "off-resonance" microwave absorption for a metallic bimaterial sensor due to eddy current heating. In these experiments, the skin depth $\delta = (2\rho/\mu\omega)^{1/2}$ is about 1 μm (μ is the permeability of the film and ρ is the electrical conductivity). The ac power loss for a thin metal film scales with ρ when $t_1 < \delta$, as is the case here.[20] Under these conditions we expect that the offsets of the absorption peaks materials should scale approximatley as $\rho\, E_1$. Eddy-current heating is reduced significantly if H_1 lies in the plane of the FMR detector film.

2. EXPERIMENTAL

The detection electronics are similar to those typical of optical chopping methods developed for photo-absorption experiments.[21] The schematic diagram is shown in Fig. 8. We monitor the deflections of the cantilever with a laser beam-bounce method. A diode laser source is focused onto the cantilever and reflected onto a split photodiode detector. This system is commonly found in commercial AFM instruments and is capable of detecting 10 picometer vibrations under ambient conditions. The microwaves are applied to the sample by placing the cantilever in close proximity to a stripline resonator driven by a microwave sweeper.

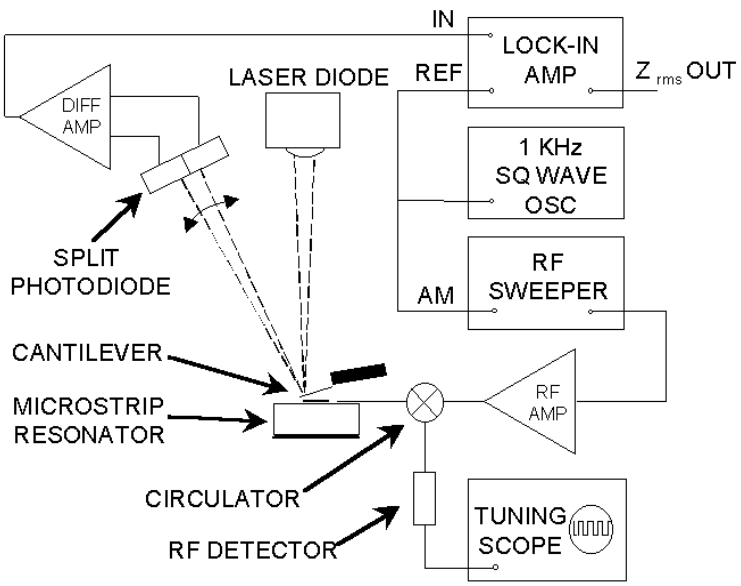

Fig. 8. Instrumentation for mechanical detection of FMR. The instrument has three main sub-systems including an AFM head, a microwave amplitude modulator or "chopper," and a tuned microstripline resonator.

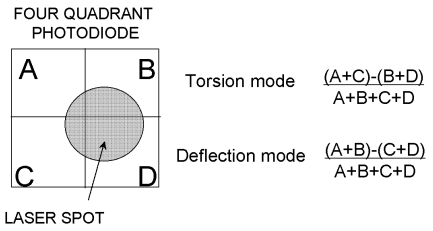

Fig. 9. Reflected laser spot on photodiode detector.

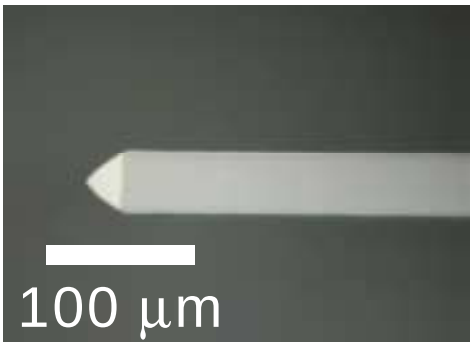

Fig. 10. Silicon cantilever coated with a NiFe film. Here, only the very tip of the cantilever is coated.

The microwave output from the sweeper is amplitude modulated by a square wave. The square wave also serves as the reference for the lock-in amplifier that measures the differences of the outputs from the split photodiode detector. The reflected wave from the microstrip resonator is monitored with the tuning scope. The microwave frequency is adjusted to obtain a minimum reflected wave amplitude as measured by the rf detector, indicating a maximum coupling of microwave power into the micostrip resonator. The cantilever deflection signal corresponds to the (C+D)-(A+B) signal, whereas the cantilever torque signal corresponding to the (A+C)-(B+D) signal (see Fig. 9). This configuration enables us to detect both the deflection and the torque signals with the same apparatus.

We prepared samples by depositing 30 nm films of either Co, NiFe alloy (81% Ni), Ni, or Au onto the flat sides of commercially available single-crystal Si cantilevers. Depositions were done in a diffusio-pump vacuum chamber with a liquid nitrogen cold trap. The base pressure was 3 x 10^{-4} Pa. The films were evaporated from alumina-coated W boats at a deposition rate of 0.15 nm/s. The cantilever dimensions were 2.5 μm x 49 μm x 449 μm with a deflection spring constant of 0.35 N/m, a deflection resonant frequency of 17 kHz, a torsion spring constant of 3.0 x 10^{-20} N·m/rad, and a torsional resonant frequency of 250 kHz. Figure 10 shows a cantilever partially coated with a NiFe film.

3. RESULTS AND DISCUSSION

3.1 Magnetization versus field (M-H) loops

Figure 11 shows the experimental configuration for measuring *M-H* loops with a microcantilever torque magnetometer (MTM).[22] Figure 12 shows two hysteresis loops for 10 nm Fe films measured with the MTM and with an alternating gradient magnetometer (AGM) for comparison purposes. In this experiment, we ramped up the sweep field H_0 to the maximum negative value of 7 mT before recording the data. The torque field H_T provided by the solenoid was kept constant at a level below 0.1 mT for the measurement. Several interesting observations were made (summarized in Table I): The torque signals decreased linearly with decreasing film thickness, i.e., magnetic volume. The magnetic moment *m* decreased from 8.9 x 10^{-10} A·m^2 for a 40 nm thick to 1.8 x 10^{-11} A·m^2 for a nominally 1 nm thick Fe film. For Fe film thickness from 40 nm to 4 nm the hysteresis loop was open, as expected, for an easy-axis hysteresis loop of a ferromagnetic film. A closer analysis of the data of the nominally 2.5 nm thick Fe film shows an open hysteresis loop with a very small coercivity H_c of about 0.08 mT. The coercivity of the 40 nm thick Fe film was 2.5 mT, whereas the 20 nm thick film showed a coercivity of 2.1 mT, and the 4 nm Fe film 0.5 mT.

These results agree with our AGM measurements performed on co-deposited samples on 6 mm x 6 mm mica substrates. Generally, the characteristic features of the thin Fe films are apparent in both sets of data. The coercivity values however, are not the same. The AGM measurement shows substantially larger coercivity values. For the 40 nm Fe film the coercivity as measured by the AGM was 4.4 mT, compared to 2.5 mT for the MTM measurement. The difference could be explained by structural changes of the Fe film prepared on mica and by the field gradient of the AGM in the direction of the easy axis of the film. For high-coercivity films, this field gradient has little effect on their magnetic measurements, but for soft magnetic films it will affect the measured hysteresis loops. In contrast, torque-field gradients have a smaller effect on our MTM measurements because the torque field is in the direction of the hard axis of the film. Also the torque field gradients are smaller in amplitude; we believe therefore that the MTM coercivity measurements are more accurate than the AGM measurements.

We conclude from the data that the SNR of our room-temperature MTM allows for measurements of Fe films with a nominally 1 nm thickness. The behavior of the film is still ferromagnetic. The total magnetic volume of this sample was calculated to be 2.2 x10 $^{-11}$ cm^3. A direct correlation of the measured loop with an AGM measurement was not possible, since the sensitivity of the available instrument was not sufficient to detect any ferromagnetic signals from Fe films with thickness less than 4 nm. The torque signal increases linearly with the applied torque field, which scales as expected with the current in the coil. We could not observe any saturation of the torque signal at higher torque fields that could be assigned to canting or out-of-plane rotation of the magnetization. We estimate that our torque fields are in the range of 0.01 to 0.57 mT. Even for a torque field as small as 0.1 mT, a SNR of 40 is obtained with our MTM instrument.

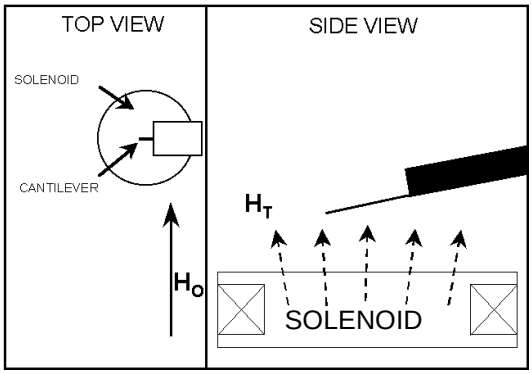

Fig. 11. Experimental configuration for magnetic torque measurements with a cantilever (from Ref. 22).

Table I : Magnetic properties of Fe films (from Ref. 22).

Fe film thickness (nm)	Magnetic volume V (cm^3)	Mag. Moment m ($A\text{-}m^2$)	Magnetization M_{60mT} (10^3 A/m)
40[1]	1.0 x 10^{-6}	1.0 x 10^{-6}	1008
40[2]	0.88 x 10^{-9}	8.9 x 10^{-10}	1008
20[1]	0.58 x 10^{-6}	6.4 x 10^{-7}	1103
20[2]	0.44 x10^{-9}	4.9 x 10^{-10}	1103
10[1]	0.28 x 10^{-6}	3.1 x 10^{-7}	1092
10[2]	0.22 x 10^{-9}	2.4 x 10^{-10}	1092
4[1]	0.10 x 10^{-6}	8.3 x 10^{-8}	807
4[2]	0.88 x10^{-10}	7.1 x 10^{-11}	807
2.5[2]	0.55 x10^{-10}	4.4 x10^{-11}	807*
1[2]	0.22 x10^{-10}	1.8 x10^{-11}	807*

[1] Alternating gradient magnetometer (AGM) measurement
[2] Microcantilever torque magnetometer measurement
Estimated value based on AGM measurements of thicker films

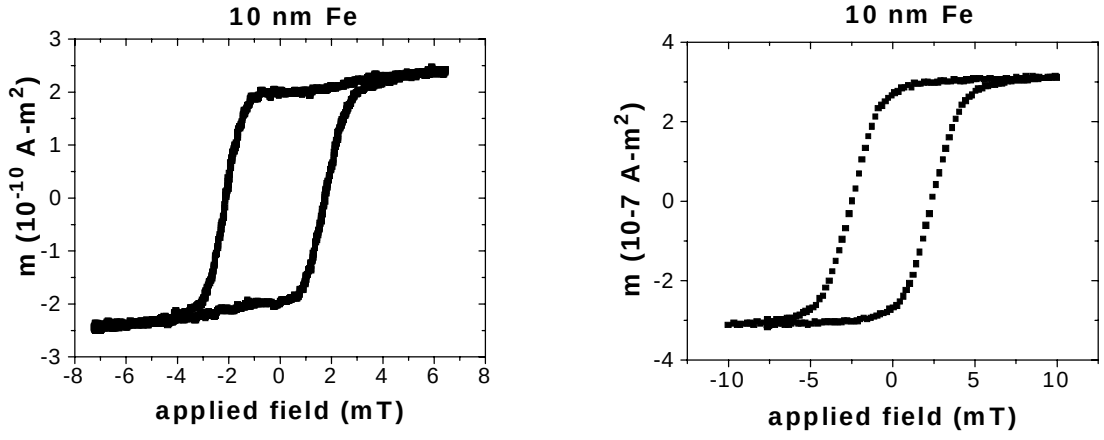

Fig. 12. M-H loops on similar Fe films measured with a MTM (left) and an AGM (right). The AGM sample was necessarily much larger than the MTM sample due to the differences in instrument sensitivities (from Ref. 22).

3.2 μRTM FMR spectra

The experimental configuration for FMR with a μRTM is shown in Fig. 13.[23] The torque T on the cantilever as measured by the lock-in amplifier is plotted versus the applied sweep field H_0. In this case about 68 μm of the cantilever was coated with a 30 nm thick NiFe film, which corresponds to a total magnetic volume of 1.1 x 10^{-10} cm^3. In order to find the torsional resonance frequency f_T of the cantilever, we swept the frequency of the oscillator providing the ac current to a torque coil prior to the measurement. The torsional frequency f_T was found to be 250.3 kHz. We used this frequency to trigger the pulse modulation of the microwave field and as reference to the lock-in amplifier. The input power to the microstrip resonator was 75 mW. The data are shown in Fig. 14. Note that the direction of the torque is reversed upon reversing sweep field as expected.

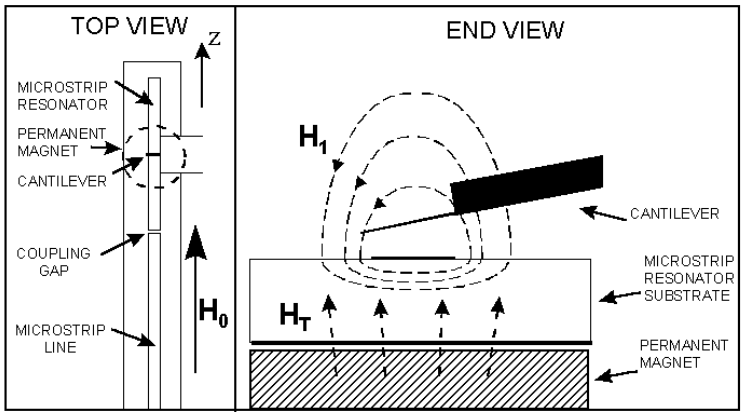

Fig. 13. Experimental configuration for FMR with a μRTM (from Ref. 23).

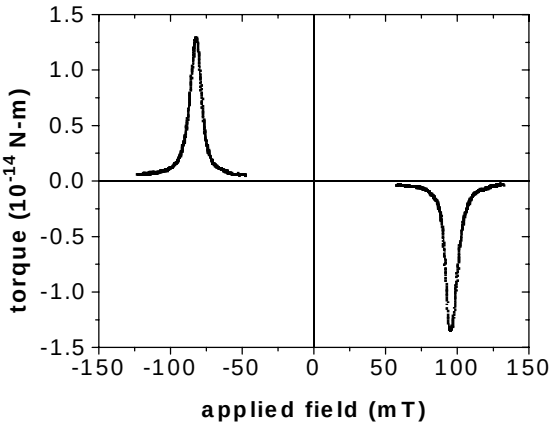

Fig. 14. Torque versus applied field measured with the μRTM for a 30 nm thick NiFe film (from Ref. 23).

We are currently developing the experimental configuration shown in Fig. 15 for FMR detection by angular momentum absorption. The results will be published elsewhere.

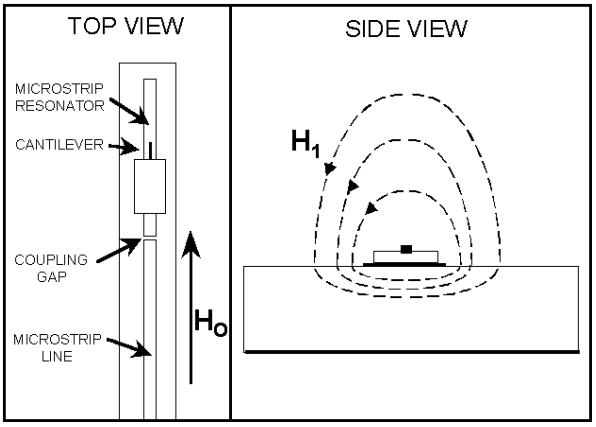

Fig. 15. Experimental configuration for FMR by angular momentum absorption. In this configuration a static torque field is not required for FMR detection. The microwave field provides a net time average torque to the sample that twists the cantilever as described in Fig.s 6 and 7.

3.3 Bimaterial mechanical calorimeter FMR spectra

The experimental configuration for FMR with a bimaterial calorimeter[21] is shown in Fig. 16. Figure 17 shows the FMR microwave absorption spectra of Co, NiFe, and Ni. The results are shown in Table II. We determined the peak locations and widths by fitting the data to Lorentzian absorption lines. Here, H_r is the resonant field, γ is the gyromagnetic constant, ΔH is the width of the resonance peak at half maximum as determined by the Lorentzian fit, and $\omega = 2\pi f$ is the microwave

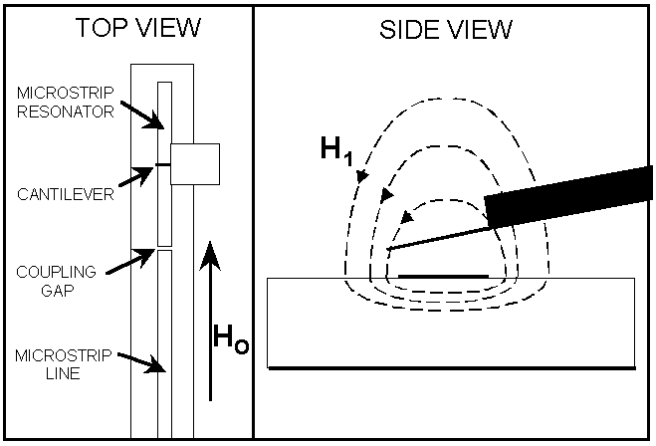

Fig. 16. Experimental configuration for FMR with a bimaterial calorimeter (from Ref. 21).

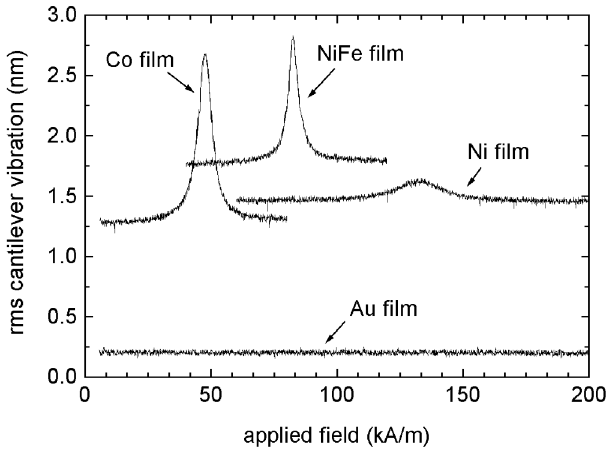

Fig. 17. Cantilever vibration versus applied field for several thin film samples measured with a bimaterial calorimeter (from Ref. 21).

Table II. Comparison of FMR data – microwave absorption versus tuned cavity detection (Ref. 21)

sample	H_r (kA/m)	ΔH (kA/m)	f (GHz)	M_{eff} (kA/m)	α	χ''
Co[1]	47.6	6.8	9.17	1260	0.014	348
Co [2]	60.6	10.4	9.88	1130	0.021	205
NiFe[1]	82.7	5.1	9.17	672	0.010	242
NiFe[2]	93.9	5.7	9.88	676	0.011	219
Ni[1]	132.9	20.0	9.17	334	0.040	26
Ni[2]	154.1	27.4	9.88	326	0.055	18

[1] microwave absorption
[2] resonant cavity
note: $\gamma = 2.31 \times 10^8$ rad/s · $(kA/m)^{-1}$

frequency. We have also included a summary of the FMR data obtained for the same samples with a conventional resonant cavity spectrometer in Table II.

Generally, M_{eff} and α agree for the two types of FMR measurements, but with some differences possibly due to the different detection methods. The resonant cavity FMR spectrometer measures the derivative of the absorption line as a function of field as opposed to the microwave absorption spectrometer described here which measures the absorption line directly. In addition, the cantilever chip has several small indentations so that some portions of the magnetic films are at an angle relative to the applied field. This also tends to broaden the FMR line as observed with the resonant cavity instrument.

4. MAGNETIC MOMENT SENSITIVITIY

4.1 The mechanical thermal limit

The Brownian motion of the cantilever due to thermal excitation fundamentally limits its ultimate sensitivity. However, there are several other sources of noise that must be reduced before the Brownian motion limit can be achieved. In particular, we have observed substantial noise contributions from the laser diode, the photodiode detector, the microwave source, room vibration, acoustic coupling, and air convection. Operating in vacuum would not only reduce viscous damping and thus increase Q but help decrease acoustic and convective noise sources as well. The Q for bare, single-crystal, silicon cantilevers can be well over 10^4. If the Brownian motion limit can be achieved and we can fabricate coated cantilevers with a Q of 10^4 then it should be possible to improve the sensitivity of MEMS magnetometers significantly.

The thermal noise can be expressed in terms of an equivalent noise on the cantilever deflection or torsion. It depends on the spring constant k_s, the mechanical quality factor Q, the resonant frequency f_o, and the thermal energy k_BT. Typical values for the experiments described in this paper are shown to the left. With an increase in Q to a value of 10^4 we expect a factor of 100 reduction in thermal noise. Cantilever geometry, material, and surface coating affect the value of Q. For very thin cantilevers, roughness and surface contamination also become important. Yasumara *et al*.[24] have performed a systematic study of these effects on the Q for cantilever deflection modes, however, a similar study on torsional modes has not yet been done.

Cantilever Deflection	Cantilever Torsion
$F_{noise} = \sqrt{\frac{2k_BTk_s}{Q f_o}}$	$T_{noise} = \sqrt{\frac{2k_BTk_s}{Q f_o}}$
$k_s = 0.2\ N/m$	$k_s = 3\cdot 10^{-8}\ N\cdot m/rad$
$f_o = 15\ kHz$	$f_o = 250\ kHz$
$Q = 200$	$Q = 250$
$F_{noise} \approx 10^{-14}\ N/\sqrt{Hz}$	$T_{noise} \approx 10^{-17}\ N\cdot m/\sqrt{Hz}$

4.2 Comparison of magnetometer magnetic moment sensitivities.

Table III summarizes reported sensitivities for several types of magnetometers. The commercial systems listed here are for typical instruments designed for routine measurements of relatively large samples. In general, these instruments have large detector volumes required for accommodating larger samples. One of the main advantages of integrating a sample with a detector, as is the case for the MEMS magnetometers discussed in this paper, is that the sample volume and the detector volume are nearly the same. It is difficult to do this with commercial systems for very small samples. In addition, some commercial systems are not well suited for measurements of low-moment samples because of electronic noise sources or instrument design. For example, a commercial torque magnetometer is very similar to a μRTM in that it measures a mechanical torque due to sample anisotropy when a torque field is applied perpendicular to the surface of the sample. However, for large commercial systems it is difficult to operate in a resonance mode since the mass of the torque arm is quite large compared to the torsional spring constant making for low resonant frequencies. It is also difficult to rotate an electromagnet quickly. Other methods have been successfully demonstrated where sample and detector are integrated in a microfrabricated measurement package. Thin films can be deposited directly onto a microstrip transmission line. Microwave transmission can then be measured as a function of applied field. This has been done both inductively as well as using the sample as the sensor if it is magnetoresistive. Finally, we refer to the long standing work on developing a magnetic resonance force microscope and integrated sample SQUID magnetometers with the potential for measuring a single electron spin flip at cryogenic temperatures.

Table III. Magnetometer sensitivity comparisons

System	Sensitivity ($A\cdot m^2$)
Commercial Systems:	
Torque magnetometer	10^{-12}
Alternating gradient magnetometer (AGM)	10^{-11}
SQUID magnetometer	10^{-11}
Fluxgate magnetometers	10^{-11}
Vibrating sample magnetometer (VSM)	10^{-9}
MR spectrometer	10^{-7}
NIST micromechanical systems (this work)	
micro resonating torque magnetometer:	
current	10^{-16}
potential MEMS optimization	10^{-18}
micromechanical FMR calorimeter:	
current	10^{-12}
potential MEMS optimization	10^{-16}
Integrated-sample stripline measurements:	
inductive[25]	10^{-13}
Magnetoresistive sensor[26,27]	10^{-15}
The "outer limits" (temperatures < 4 K)	
magnetic resonance force microscope (predicted)[28]	10^{-23}
1 μm SQUID loop at 4 K (measured)	10^{-21}
0.1 μm SQUID loop at 100 mK (predicted)[29]	10^{-23}

units: 1 $\mu_B = 10^{-23}\ A\cdot m^2$, $(10\ nm)^3$ Co = $10^{-16}\ A\cdot m^2$[1], and 1 emu = $10^{-3}\ A\cdot m^2$

5. METROLOGY APPLICATIONS

We conclude with a discussion of some relevant applications that should benefit form MEMS based magnetometers and the technical challenges that must be overcome for these applications to be realized. Currently we are considering the following:

5.1 A new way to measure M_s by combining angular momentum absorption and power absorption measurements

From Eq. (3), we see that a gyromagnetic constant for a given material must be independently determined in order to use FMR to measure M_s. We propose a way out of this requirement by combing the angular momentum and power absorption measurements described above. We can measure both the of these quantities in the same apparatus without changing the experimental parameters or the sample film. The absorbed power results in a deflection of the cantilever tip. Simultaneously, the torque on the sample results in a torsion of the cantilever beam. By measuring the ratio P_{res}/T_{res} we may be able to eliminate the need for the independent γ measurement. However, this will require a broadband microwave source. The microstrip resonator we currently use provides a sufficiently large H_1. Replacing the resonator with a microstrip transmission line with broadband characteristics might work, but a reduction in H_1 may adversely affect the SNR.

5.2 A new type of microwave microscope based on a scanning FMR cantilever

All three FMR MEMS magnetometers described in this paper have potential as a proximity probe of the microscopic magnetic fields near microwave devices. The cantilever response for each of the detection modes described above is proportional to H_1^2, and thus such a probe measures the local power density above an active circuit. The spatial resolution of the scanning probe depends on its sensitivity to changes in magnetic field that in turn depends on the magnetic moment sensitivity of the detection system. With modest improvements in cantilever design and operation in vacuum, it should be possible to achieve sub-micrometer resolution. The technical challenge here is to develop ways to put a sub-micrometer FMR probe on the end of an AFM tip.

5.3 Smart substrates for *in-situ* monitoring of magnetic film properties during deposition or post-processing steps

The growth conditions for making ultra-thin films and thin film multilayers are critical to maintain product uniformity. Typically, film deposition is monitored *ex-situ* with B-H loopers that determine the $M_s t$ product for the film. There are no standard reference materials with magnetic moments similar to these samples. Rather, one must rely on the linearity of preamplifiers over several decades in order to relate the moment of an ultra-thin film to a much larger magnetic reference sample. We propose developing disposable smart substrates based on MEMS where a reference film is deposited onto a wafer of μRTMs. The wafer is characterized in a large sample magnetometer and then diced into individual chips for *in-situ* testing. The magnetization of the film is determined by the ratio of the torques measured before and then after deposition or processing. Once the measurements are completed, the μRTM substrate would be discarded.

6. REFERENCES

1. M. J. Naughton, J. P. Ulmet, A. Narjis, S. Askenazy, M. V. Chaparala, A. P. Hope, "Cantilever magnetometry in pulsed magnetic fields," Rev. Sci. Instrum. **68**, pp. 4061-4065, 1997.
2. C. Rossel, M. Willemin, A. Grasser, H. Bothuizen, G. I. Meoijer, H. Keller, "Torsion cantilever as magnetic torque sensor," Rev. Sci. Instrum. **69**, pp. 3199-3203, 1998.
3. G. P. Heydon, A. N. Farley, S. R. Hoon, M. S. Valera, S. L. Thomlinson, "Resonant torque magnetometry: a new *in-situ* technique for determining the magnetic properties of MFM tips," IEEE Trans. Mag. **33**, 4059-4061, 1997.
4. R.E. Mihailovich, J. M. Parpia, "Low temperature mechanical properties of boron-doped silicon," Phys. Rev. Lett. **68**, pp. 3052-3055, 1992.
5. R. D. Biggar, J. M. Parpia, "High-Q oscillator torque magnetometer," Rev. Sci. Instrum. **69,** pp. 3558-3562, 1998.
6. M. Todorovic and S. Shultz, "Miniature high-sensitivity quartz tuning fork alternating gradient magnetometry," Appl. Phys. Lett. **73**, pp. 3595-3597, 1998.

7. J. Morrillo, Q. Su, B. Panchapakesan, M. Wuttig, and D. Novotny, "Micromachined silicon torsional resonator for magnetic anisotropy measurement," Rev. Sci. Instrum. **69**, pp. 3908-3912, 1998.
8. S. Chikazumi, *Physics of Magnetism*, Kreiger Publishing, Malabar, Florida, 1964.
9. B. Heinrich, A. S. Arrott, J. F. Cochran, K. B. Urquhart, K. Myrtle, Z. Celinski, Q. M. Zhong, "*In-situ* techniques for studying epitaxially grown layers and determining their magnetic properties," Mat. Res. Soc. Symp. Proc., **151**, pp. 177-188, 1989.
10. R. J. Roark and W. C. Young, *Formulas for Stress and Strain*, McGraw Hill, New York, 1975.
11. L. D Landau, E. M. Lifshitz, *Theory of Elasticity*, Pergamon Press, New York, 1970.
12. C. Lupien, B. Ellman, P. Grütter, L. Taillefer, "Piezoresistive torque magnetometry below 1 K," Appl. Phys. Lett. **74,** pp. 451 – 453, 1999.
13. C. Rossel, P. Bauer, D. Zech, J. Hofer, M. Willemin, H. Keller, "Active microlevers as miniature torque magnetometers," J. Appl. Phys. **79**, pp. 8166-8173, 1996.
14. S. Chikazumi, *Physics of Magnetism*, Kreiger Publishing, Malabar, Florida, pp. 333-348, 1964.
15. B. Heinrich and J. F. Cochran, "Ultrathin metallic magnetic films: magnetic anisotropies and exchange interactions," Avances in Physics **42,** pp. 523-639, 1993.
16. P. Kabos, C. E. Patton, M. O. Dima, D. B. Church, R. L. Stamps, and R. E. Camely, "Brillouin light scattering on Fe/Cr/Fe thin-film sandwiches," J. Appl. Phys. **75**, pp. 3553-3563, 1994.
17. P. Kabos, *High Frequency Processes in Magnetic Materials*, Chapter 1, Eds. G. Srinivasan and A. Slavin, World Scientific, 1995.
18. J. M. Nash, P. Kabos, R. Staudinger, C. E. Patton, "Phase profiles of microwave magnetic envelope solitons," J. Appl. Phys. **84**, pp. 2689-2699, 1998.
19. J. R. Barnes, R. J. Stephenson, C. N. Woodburn, S. J. O'Shea, M. E. Welland, T. Rayment, J. K. Gimzewski, and Ch. Gerber, "A femtojoule calorimeter using micromechnaical sensors," Rev. Sci. Instrum. **65**, pp. 3793-3798, 1994.
20. J. Booth, National Institute of Standards and Technology, private communication: The surface resistance of a metallic film, assuming that losses are dominated by eddy current heating, is $Z \approx \rho/t$ given $t << \delta$. We have verified this result based on first principles and note that one must further require that the reflectivity of the film be close to unity. As the film thickness is decreased and its reflectivity drops well below unity the relation $Z \approx \rho/t$ is no longer valid.
21. J. Moreland, M. Löhndorf, P. Kabos, and R. D. McMichael, "Ferromagnetic resonance spectroscopy with a micromechanical calorimeter," accepted for publication in Rev. Sci. Instrum., August 2000.
22. M. Löhndorf, J. Moreland, P. Kabos, and N. Rizzo, "Microcantilever torque magnetometry of thin magnetic films," J. Appl. Phys. **87**, pp. 5995-5997, 2000.
23. M. Löhndorf, J. Moreland, and P. Kabos, "Ferromagnetic resonance detection with a torsion mode atomic force microscope," Appl. Phys. Lett. **76**, pp. 1176-1178, 2000.
24. K. Y. Yasumara, T. D. Stowe, E. M. Chow, T. Pfafman, T. W. Kenny, B. C. Stipe, and D. Rugar, "Quality factors in micron and submicron thick cantilevers," J. Microelectromechanical Systems **9**, pp. 117-125, 2000.
25. S. Zhang, J. B. Sokoloff, and C. Vittoria, "Measurements and simulations of micron size coplanar waveguides," J. Appl. Phys. **81**, pp. 5076-5078, 1997.
26. R. H. Koch, J. G. Deak, D. W. Abraham, P. L. Trouilloud, R. A. Altman, Yu Lu, W. J. Gallagher, R. E. Scheuerlein, K. P. Roche, and S. S. P. Parkin, "Magnetization Reversal in Micron-Sized Magnetic Thin Films," Phys. Rev. Lett. **81**, pp. 4512-4515, 1998.
27. S.E. Russek, J.O. Oti, S. Kaka, and E.Y. Chen, "High-speed characterization of submicrometer giant magnetoresistive devices," J. Appl. Phys. **85**, pp. 4773-4775, 1999.
28. J.A. Sidles, J. L. Garbini, K. J. Bruland, D. Rugar, O. Zügar, S. Höen, C. S. Yannoni, "Magnetic resonance force microscopy," Rev. Mod. Phys. **67**, 249-265, 1995.
29. M. Ketchen, D. J. Pearson, K. Stawaisz, C. K. Hu, A. W. Kleinsasser, T. Brunner, C.Cabral, V. Chandrashekhar, M. Jaso, M. Manny, K. Stein, and M. Bhushan, "Octagonal washer dc SQUIDs and integrated susceptometers fabricated in a planarized sub-μm Nb-AlO_x-Nb technology," IEEE Trans. Appl. Supercond. **3**, pp. 1795-1799, 1993.